Available online at www.sciencedirect.com
SCIENCE DIRECT®
Computational Materials Science 36 (2006) 60–64
COMPUTATIONAL MATERIALS SCIENCE
www.elsevier.com/locate/commatsci

Atomistic simulation of the influence of pressure on dislocation nucleation in bcc Mo

D.S. Xu [a,*], R. Yang [a], J. Li [b], J.P. Chang [c], H. Wang [a], D. Li [a], S. Yip [c]

[a] Titanium Alloy Laboratory, Institute of Metal Research, Chinese Academy of Sciences, Shenyang 110016, China
[b] Department of Materials Science and Engineering, Ohio State University, 2041 College Road, Columbus, OH 43210, USA
[c] Department of Nuclear Engineering, Massachusetts Institute of Technology, 77 Massachusetts Avenue, Cambridge, MA 02139, USA

Received 17 September 2004; accepted 15 July 2005

Abstract

Molecular dynamics simulations were carried out to investigate the pressure dependence of homogeneous defect nucleation behavior in bcc Mo. The crystal was sheared on the $(1\bar{1}0)$ $[11\bar{1}]$ slip system under different confining pressures. The defect nucleation stress was found to increase as the confining pressure increases. Dislocation loop was nucleated when sheared under hydrostatic compression, while Martensitic transformation was found to occur when sheared under sufficient hydrostatic tension. Atomistic details of the nucleation processes are analyzed and the influence of pressure on the nucleation dynamics of dislocations has been studied. Analysis was made with the help of the energetics of generalized stacking faults when the crystal was deformed statically under different hydrostatic pressure in a highly controlled manner.

Keywords: Dislocation; Nucleation; Martensite; Molecular dynamics; bcc; Mo; Pressure

1. Introduction

Much evidence shows that non-glide components of stress on a given slip system may have important effect on the dislocation or twinning behavior of bcc metals [1–4]. Three distinct non-glide shear stress have been identified to affect the glide of $1/2\langle 111\rangle$ screw dislocations and a criteria including the effects of these stress components was formulated, which formed a basis for flow relations in continuum analysis [2]. When polycrystalline metals are deformed, even though the stress applied to the sample is quite simple, such as uniaxial tension or compression, the stress conditions inside each grain are different, due to the effects of the grain boundary, anisotropy of elastic properties and mutually-accommodating plastic deformation. The stress is more complicated near the grain boundary regions and triple junctions. These locations are usually the nucleation sites of cracks when the sample was over loaded. In the case of nanoindentation, the material beneath the indenter will deform under large compressive stress up to tens of GPa [5,6]. The crack tip region in a solid under tension is another important example of multi-axial loading. The stress there can be separated into hydrostatic tension and a tension or shear component. The stress at the crack tip may reach the level for homogeneous nucleation of defects. It has been shown by first principles calculations that the strength of bcc Fe, which had instability to fcc phase through the Bain transformation, is strongly influenced by hydrostatic stress [7]. The strength was increased by the triaxial tension. Thus, the influences of confining stresses to the nucleation of

* Corresponding author. Tel.: +86 24 23971946; fax: +86 24 23891320.
E-mail address: dsxu@imr.ac.cn (D.S. Xu).

0927-0256/$ - see front matter © 2005 Elsevier B.V. All rights reserved.
doi:10.1016/j.commatsci.2005.07.003

defects under such extreme conditions are important to the understanding of the deformation of materials.

It was found recently that the defect nucleation behavior of bcc Mo lattice when sheared on the $(1\,1\,2)$ $[\bar{1}\,\bar{1}\,1]$ twinning system can be significantly altered due to the application of confining pressure [4]. Deformation twin is nucleated when the crystal is sheared under tension, while dislocation is nucleated if the crystal is sheared under hydrostatic compression. It is therefore interesting to know what will be the effects of confining pressure on the defect nucleation behavior when the lattice was sheared on the slip system of bcc Mo.

In this work, molecular dynamics simulation was carried out to study the effects of confining pressure on the nucleation of dislocation or other defect, when the lattice was sheared on the $(1\,\bar{1}\,0)$ $[1\,1\,\bar{1}]$ slip system in perfect bcc Mo. The generalized stacking fault energy was calculated under different confinement to investigate the influence of the constraint on the shear strength of the lattice. Mo is chosen for this research not only because it is a good bcc model material, it has also important space application and may subject to both creep and shock loading, so that to understand its behavior also has some practical significance.

2. Simulation method and setup

Molecular dynamics simulation was carried out with constant strain rate loading using the Finnis–Sinclair second-moment potential for bcc molybdenum [8]. Simulation cells containing up to 0.4 million atoms were employed in the calculations, with periodic boundary condition (PBC) in all three directions. Relatively large simulation cell is chosen to let the nucleated dislocation loop or Martensitic lath have the right boundary condition in the matrix, so that their dynamics is not destroyed by the image interaction due to the PBC. Shear displacements were imposed along $[1\,1\,\bar{1}]$ direction on $(1\,\bar{1}\,0)$ plane; the confining pressure being adjusted by changing the lattice parameter. All simulations were started at temperature of 1 K, with temperature rescaling through a first-order feedback control scheme to remove the significant heat generated by plastic deformation. The shear strain rate ranged from 2×10^{6} to $10^{10}\ \mathrm{s}^{-1}$.

The simulation cell was chosen to be multiples of an elementary cell as shown in Fig. 1, in gray lines. The latter is spanned by $\mathbf{a}_1 = [1\,1\,\bar{1}]a_0/2$, $\mathbf{a}_2 = [\bar{1}\,1\,0]a_0$ and $\mathbf{a}_3 = [1\,1\,1]a_0/2$ and contains two atoms. The slip plane $(1\,\bar{1}\,0)$ is the plane spanned by $\mathbf{a}_1$ and $\mathbf{a}_3$. Shear deformation is applied on $(1\,\bar{1}\,0)$ plane along $[1\,1\,\bar{1}]$ direction, $\mathbf{a}_1$.

The generalized stacking fault energy was calculated with the lattice sheared between only two adjacent layers. No relaxation in other layers and other directions was allowed.

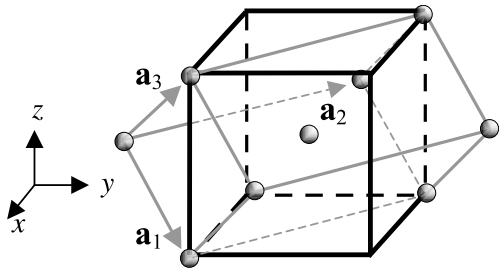

Fig. 1. Elementary cell with basis vectors $\mathbf{a}_1$, $\mathbf{a}_2$, $\mathbf{a}_3$ corresponding to vectors in the $[1\,1\,\bar{1}]$, $[\bar{1}\,1\,0]$ and $[1\,1\,1]$ directions, respectively. The bcc unit cell is delineated by the thick lines. Dislocation shear is on the $\mathbf{a}_1\times\mathbf{a}_3$ plane along $\mathbf{a}_1$ direction, i.e., the slip system of the bcc metal: $[1\,1\,\bar{1}]$ direction on $(1\,\bar{1}\,0)$ plane (reproduced from Ref. [4]).

3. Results and discussion

3.1. Confining dependence of nucleation stress of defects

Fig. 2 shows the nucleation stress of defects in perfect bcc Mo when the crystal is sheared on the $(1\,\bar{1}\,0)$ $[1\,1\,\bar{1}]$ slip system. The x-axis is the ratio of the length of the simulation box when the system is under confining to that under zero pressure, which is an indication of the confining pressure applied to the system. It can be seen from the plot that the yield stress increases with the increasing of the confining pressure (decreasing of lattice parameters). This trend is similar to the relation of $(1\,1\,2)$ $[\bar{1}\,\bar{1}\,1]$ twinning shear strength and confining pressure, but the curvature here is negative, showing a weaker dependence on compression and a stronger dependence on tension. The yield strain increases also with increasing confining pressure.

The increase of shear strength with confining pressure can be understood by the change of generalized stacking fault energy with the confining pressure. Fig. 3 shows

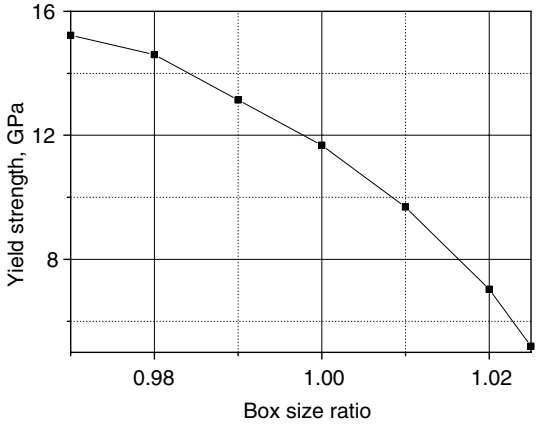

Fig. 2. Confining dependence of the yield strength of lattice sheared on the $(1\,\bar{1}\,0)$ $[1\,1\,\bar{1}]$ slip system. The confining pressure was controlled by adjusting the size of the simulation box, and x-axis here represents the ratio of the box size to that under zero pressure.

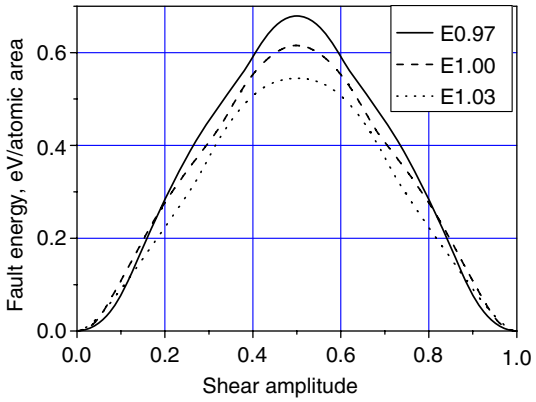

Fig. 3. Change of generalized stacking fault energy with confining pressure on the $(1\bar{1}0)$ $[11\bar{1}]$ slip system. The E0.97, E1.00 and E1.03 correspond to the fault energy when the lattice was sheared under compression, zero pressure and tension.

the shear fault energy curve when the lattice parameter is at 0.97, 1.00 and 1.03 of its equilibrium value, showing the effects of compression or tension on the lattice resistance to the defect nucleation. It can be seen that the energy barrier of shearing the lattice on the $(1\bar{1}0)$ $[11\bar{1}]$ slip system is higher when the lattice is sheared under compression than under tension. The slope of the energy curve around the first inflection point for shearing under compression is much larger than that under tension; this gives a larger restoring force from the lattice, corresponding to larger shear strength under compression. The first inflection point of the curve in Fig. 3 under compression corresponds to larger shear amplitude than other cases (e.g., 0.15 for $0.97a_0$ vs. 0.12 for $1.00a_0$), suggesting a higher shear yield strain of the compressed lattice. It can also be seen from the slope changes in the curve of Fig. 3 that the shear modulus becomes lower when the lattice was sheared under tension for a shear displacement of a few percent. This lowering of the modulus caused the instability of the bcc lattice and formation of the Martensite with the orthorhombic structure. It should be noted that on the curves in Fig. 3, there is a second inflection point around 30% of the shear displacement along [1 1 1] direction, while it is absent in the BOP and DFT calculation [9]. This is due to the potential cutoff used in the Finnis–Sinclair potential, which is associated with the lattice properties through the fitting procedure of the parameter in the potential. Although the second inflection point appeared at much larger shear deformation than that when the lattice lost its stability (at around the first inflection point), it may influence the final structure of the defect nucleated during the shear deformation. More calculation using DFT or BOP might be needed to clarify the final structure of the Martensite generated when the lattice was sheared under hydrostatic tension.

3.2. Dynamic yielding during confined shear

Fig. 4 shows the stress–strain curve when the lattice was sheared under hydrostatic compression of 1% and tension of 2.5%. It can be seen that the lattice yielded at a shear strain of about 10% when it was under 1% compression, but the yield strain is about 3% under 2.5% hydrostatic tension. The two curves behave differently after yielding, indicating nucleation of different types of defects when the lattice was sheared under different confining pressure. The curve under tension shows some oscillation after yielding, as can be seen from the following analysis. This corresponds to the nucleation of Martensite in the bcc matrix.

3.3. Defect configuration produced by shearing under compression

Under hydrostatic compression, a dislocation loop is nucleated when the lattice shear reaches a critical value. Segments of the expanding loop travel at a high speed due to the high level of stress. Fig. 5 shows configuration of edge and screw segments of the nucleated dislocation loop. The bonds between first and second nearest neighbor atoms were shown in edge part (Fig. 5b), in order to

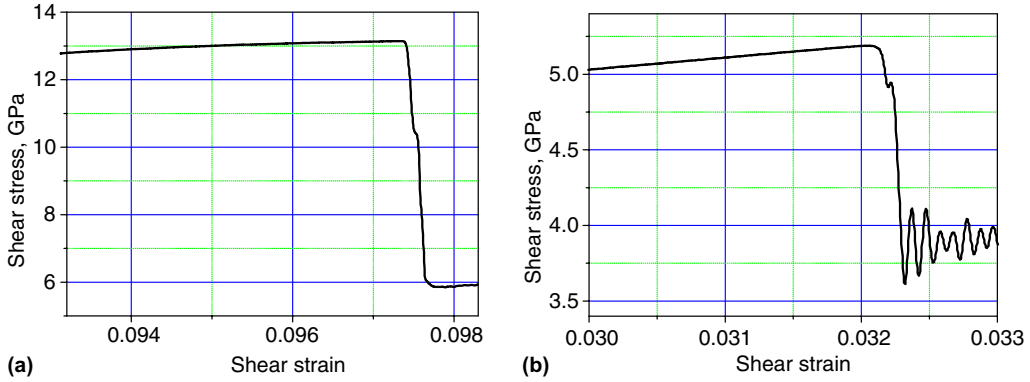

Fig. 4. Stress–strain relation for the lattice sheared under (initially) hydrostatic compression of 1% (a) and tension of 2.5% (b).

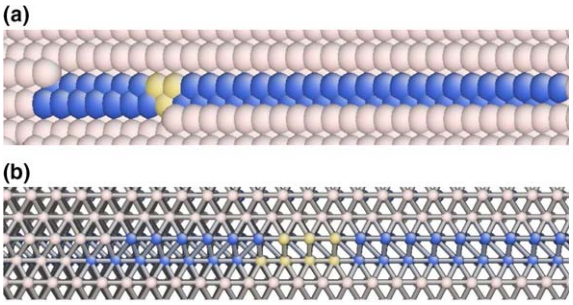

Fig. 5. Planar core configuration for screw (a) and edge (b) portion of dislocation loop nucleated. The gray, blue and yellow colors show the atoms with coordination number (including first and second nearest neighbors in bcc lattice) 14, 13 and 12, respectively. Bonds between neighboring atoms in edge dislocation are used to show the misregistry between atomic planes in the core region [10]. (For interpretation of the references in colour in this figure caption, the reader is referred to the web version of this article.)

show the misregistry between atomic layers in the dislocation core region. The screw dislocation core is shown using the color encoding by coordination number of each atom [10]. The dislocation here shows planar character in both the edge and screw orientation, in contrast to those of non-planar behavior in some other simulation [2,11]. One of the reason is due to the dislocation here was nucleated under high level of stress and subsequently moved in a very high speed. It is shown from the previous simulation that the dislocation core shows its non-planar character when it stops, but it is flattened once it starts to move [12]. Another reason of the planar core structure may be due to the interaction between different dislocation segments in the loop. The two opposite screw portions in the same loop on the same slip plane will impose on each other a shear force field in the plane of the loop, which would increase the fraction of screw partial in the loop plane, that favors the planar configuration of the screws. The larger compressive force perpendicular to the slip plane generated by the lattice shearing may also contribute to the contraction of the core in the direction perpendicular to the slip plane.

3.4. Martensitic transformation by shear under hydrostatic tension

When the hydrostatic tension exceeds about 1%, the lattice no longer yields by nucleation of dislocation loop, but accommodates the plastic deformation by local martensitic transformation. Fig. 6 is a snapshot of the shearing process, showing a lath of Martensite (convex lens shape as it was nucleated) in the bcc lattice. The volume containing yellow atoms with a lower coordination number of 12 is an orthorhombic Martensite phase formed by shearing of the simulation box along the x-axis. The density of the transformed part is lower than the matrix to accommodate the lattice expansion due

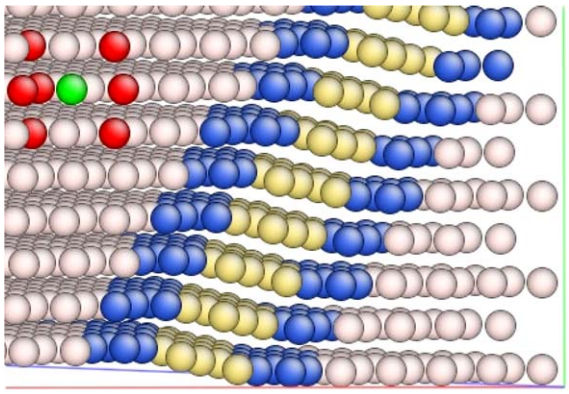

Fig. 6. Martensite formed by shearing under tension. The red, green and blue axes correspond to the $\mathbf{a}_1$ $\mathbf{a}_2$ and $\mathbf{a}_3$ axes in Fig. 1. The shear direction of the box is parallel to the red axis, along $\mathbf{a}_1$, on the plane spanned by the red and blue axes. The gray, blue and yellow atoms have coordination number of 14, 13 and 12 respectively. The red atoms on the upper left corner show a bcc elementary cell, with a green atom as its center. The transformed part designated by yellow atoms has a lattice close to orthorhombic structure. (For interpretation of the references in colour in this figure caption, the reader is referred to the web version of this article.)

to the hydrostatic tension. The volume expansion due to the martensitic transformation is about 20% for shearing under 3.2% hydrostatic tension. This is comparable to an earlier calculation for iron, which shows about 8% volume expansion after bcc to fcc transformation [13], but in contrast with experimental observation for iron. The experimental volume expansion for Fe alloys is about 4% from fcc to bcc Martensite [14,15]. The difference in the amount of the lattice expansion between previous and the calculation here may partially be due to the difference in stress state. In the calculation here, the lattice is in large tension of, say 3.2%, in each direction, so the Martensite is still under tension even after the transformation, and it is naturally bigger in volume than that in unstressed case. In the experimental case, when Martensite is formed, it expands in volume, so that subjected to compressive stress by the matrix, that may be the reason why the measured volume expansion is smaller than that in the calculation [13–15]. If we deduced the influence of the tensile stress on the density, we may estimate the volume expansion of the lattice due to the transformation to be similar with that of previous calculation for iron [13].

The habit plane of the Martensite formed is somewhat sensitive to the geometry of the simulation box, i.e., the length ratio of different axes of the box, i.e., it depends on the total stress. The local lattice shear direction in each transformation is similar, so that give the same lattice structure of Martensite. In one case the habit plane of transformed lath is close to $(1\,\bar{7}\,2)$ of the bcc matrix. The shear direction is about [1 2.5 1.7]. The lattice plane rotation due to the transformation is about 17°. This makes the initial 71° lattice into almost right

angle. The Martensite formed has a structure close to face centered orthorhombic lattice. In the center part of the lath, each angle is close to 90°, with deviation of a few degrees. The b/a ratio is 0.97 and c/a ratio is about 1.03. This martensitic structure is different from fcc, with a deviation of $\pm 3\%$ for axial ratio. The larger c-axis of the orthorhombic lattice may be due to the larger tensile stress along the c direction, since the c is along the Martensite lath; there is not much stress relaxation in this direction.

The density of the Martensite is lower than that of the bcc phase. This is in contrast to the general belief that fcc may have a higher density than bcc phase. The density of the equilibrium fcc Mo is higher than that of bcc phase using the same potential, so that the martensitic phase here may be another phase of the Mo under hydrostatic tension. Further ab initio type calculation may be needed to test the stability of the low density orthorhombic or fcc phase of Mo. It should be noted that the value given here is measured in the dynamic simulation; more accurate ones can only be obtained by performing careful relaxation of the transformed lattice.

The choice of potential may have important influence on the deformation behavior of the system. Recent calculations for molybdenum with different interatomic interactions show that for the central force many body potential, the generalized stacking fault energy deviate from that calculated using different bond-order potentials and density functional based method when the shear displacement exceeds 10% of the Burgers vector in $[1\,1\,1]$ direction, and the core structure of dislocations are also different [9,2]. Some further calculation using other potential, such as bond order potential or first principles calculation might be interesting to clarify the physical origin of this transformation on the electronic structure level.

4. Conclusion

Molecular dynamics simulation using the Finnis-Sinclair potential has been carried out to study the effect of confining pressure on the nucleation behavior of defects in bcc molybdenum perfect crystal sheared on $(1\bar{1}0)$ $[1\,1\,\bar{1}]$ slip system. The following conclusions can be drawn:

(1) Confining pressure has a crucial influence on the nucleation of defects when the lattice is sheared on the slip system. Dislocation is nucleated when the lattice is sheared under compression or small tension, Martensitic transformation occurs when the lattice is sheared under sufficiently large hydrostatic tension.
(2) The shear strength of perfect bcc lattice when sheared on the $(1\bar{1}0)$ $[1\,1\,\bar{1}]$ slip system increases with the increase of the confining pressure, as a result of increasing lattice restoring force when the lattice is compressed, as can be delineated by the change of the generalized stacking fault energy profile when pressure is applied to the system.

Acknowledgements

The supports of the Ministry of Science and Technology of China under Grant No. TG2000067105 and the Natural Science Foundation of China under Grant No. 50471079 are gratefully acknowledged. D.S. Xu acknowledges the support of K.C. Wong Fellowship for his visit to MIT.

References

[1] V. Vitek, M. Mrovec, R. Gröger, J.L. Bassani, V. Racherla, L. Yin, Mater. Sci. Eng. A 387 (2004) 138.
[2] V. Vitek, M. Mrovec, J.L. Bassani, Mater. Sci. Eng. A 365 (2004) 31.
[3] K. Ito, V. Vitek, Philos. Mag. A 81 (2001) 1387.
[4] D.S. Xu, J.P. Chang, J. Li, R. Yang, D. Li, S. Yip, Mater. Sci. Eng. A. 387 (2004) 840.
[5] K.J. Van Vliet, J. Li, T. Zhu, S. Yip, S. Suresh, Phys. Rev. B 67 (2003) 104105.
[6] J. Li, K.J. Van Vliet, T. Zhu, S. Yip, S. Suresh, Nature 418 (2002) 307.
[7] D.M. Clatterbuck, D.C. Chrzan, J.W. Morris Jr., Scr. Mater. 49 (2003) 1007.
[8] M.W. Finnis, J.E. Sinclair, Philos. Mag. A 50 (1984) 45; Philos. Mag. A 53 (1986) 161.
[9] M. Mrovec, D. Nguyen-Manh, D.G. Pettifor, V. Vitek, Phys. Rev. B 69 (2004) 094115.
[10] J. Li, Model. Simul. Mater. Sci. Eng. 11 (2003) 173.
[11] J.P. Chang, Ph. D. Thesis, MIT, 2003.
[12] J.P. Chang, J. Li, Private communication, 2001.
[13] R. Najafabadi, S. Yip, Scr. Metall. 17 (1983) 1199.
[14] I. Karaman, H. Sehitoglu, H.J. Maier, M. Balzer, Met. Mater. Trans. A 29 (1998) 427.
[15] R. Neu, H. Sehitoglu, Acta Metall. Mater. 40 (1992) 2257.